to bind to NK_1 receptors with high affinity and selectivity and applied to in vivo imaging of human brains (*20–22*).

^{18}F-fluoroethyl-SPA-RQ (^{18}F-FE-SPA-RQ) was recently developed as a radioligand for the measurement of NK_1 receptors (*23*). It is the fluoroethyl analog of ^{18}F-SPA-RQ and was designed for brain imaging with reduced radioactive accumulation in bone by slowing the rate of defluorination. ^{18}F-FE-SPA-RQ has higher affinity for NK_1 receptors than does ^{18}F-SPA-RQ (human NK_1 inhibitory concentration of 50% [IC_{50}] = 17 and 67 pM for ^{18}F-FE-SPA-RQ and ^{18}F-SPA-RQ, respectively), and a small-animal PET study has been performed using ^{18}F-FE-SPA-RQ (*24*). In the present study, we aimed to quantify NK_1 receptor binding in the human brain using ^{18}F-FE-SPA-RQ with arterial blood sampling and also to validate noninvasive methods for the quantification without arterial blood sampling.

MATERIALS AND METHODS

Subjects

A total of 7 healthy male subjects (age range, 20–31 y; mean ± SD, 24.6 ± 4.0 y) participated in this study. All subjects were free of any somatic, neurologic, or psychiatric disorders, and they had no history of current or previous drug abuse. After we described the study to the participants, written informed consent was obtained. The study was approved by the Ethics and Radiation Safety Committee of the National Institute of Radiologic Sciences, Chiba, Japan.

Radioligand

The NK_1 receptor antagonist SPA-RQ (molecular weight, 450M) was labeled with the positron emitter ^{18}F (half-life, 109.8 min). Details of the precursor compound, radiosynthesis, and quality control were described previously (*23,25*). Briefly, ^{18}F-FCH_2CH_2Br was prepared from ^{18}F-F^- and 2-bromoethyl triflate and purified by distillation. ^{18}F-Fluoroalkylation of the deprotonated phenolic hydroxyl group in the precursor with FCH_2CH_2Br in dimethyl formamide was performed at 120°C for 10 min. The resultant ^{18}F-FE-SPA-RQ was purified by preparative high-performance liquid chromatography (HPLC). The final product was formulated in saline solution (10 mL) containing polysorbate 80 (75 μL).

PET Procedure

A PET scanner system (ECAT EXACT HR+; CTI-Siemens) was used for all subjects, and a head restraint was used to minimize head movement. A transmission scan for attenuation correction was performed using a ^{68}Ge–^{68}Ga source, and a dynamic PET scan was performed after a 1-min intravenous slow-bolus injection of 210.2–228.8 MBq (221.6 ± 6.7 MBq) of ^{18}F-FE-SPA-RQ. Specific radioactivity of ^{18}F-FE-SPA-RQ was 281.8–487.7 GBq/μmol (355.6 ± 68.7 GBq/μmol). Brain radioactivity was measured from 0 to 90 min (1 min × 10, 2 min × 15, 5 min × 10), from 120 to 180 min (5 min × 12), from 210 to 270 min (5 min × 12), and from 300 to 330 min (5 min × 6). MR images of the brain were acquired with a 1.5-T MRI scanner (Gyroscan NT; Philips). T1-weighted images were obtained at 1-mm slices.

Arterial Blood Sampling and Metabolite Analysis

To obtain the arterial input function, arterial blood samples were taken manually 49 times during PET. Each of the blood samples was centrifuged to obtain plasma and blood cell fractions, and the concentrations of radioactivity in whole blood and in plasma were measured.

The percentage of unchanged ^{18}F-FE-SPA-RQ in plasma was determined by HPLC in 29 of the total blood samples. Acetonitrile was added to each plasma sample, and samples were centrifuged. The supernatant was subjected to radio-HPLC analysis using an XBridge Prep C18 column (Waters) (mobile phase, 6:4 90% acetonitrile:50 mM phosphoric acid). The plasma input function was defined as the radioactivity of plasma multiplied by the percentage of unchanged radioligand. Plasma protein binding was not determined in the present study.

Regions of Interest

All MR images were coregistered to the PET images using a statistical parametric mapping (SPM2) system. Regions of interest were drawn manually on summated PET images with reference to coregistered MRI and were defined for the caudate head; putamen; parahippocampal region; occipital, temporal, frontal, and anterior cingulate cortices; thalamus; and cerebellum, according to our previous study (*26*). The parahippocampal region included the hippocampus, posterior part of the parahippocampal gyrus, and uncus including the amygdala. Regional radioactivity was calculated for each frame, corrected for decay, and plotted versus time.

Kinetics Model of ^{18}F-FE-SPA-RQ

The 3-compartment model (3CM) with 4 first-order rate constants was used to describe the kinetics of ^{18}F-FE-SPA-RQ in the brain. The 3 compartments were defined as follows: C_P, the radioactivity concentration of unchanged radioligand in plasma (arterial input function); C_{ND}, the radioactivity concentration of nondisplaceable radioligand in the brain, including nonspecifically bound and free radioligand; and C_S, the radioactivity concentration of radioligand specifically bound to receptors. The rate constants K_1 and k_2 represent the influx and efflux rates for radioligand diffusion through the blood–brain barrier, respectively. The rate constants k_3 and k_4 are the radioligand transfers between the compartments for nondisplaceable and specifically bound radioligand. This model can be described by the following equations:

$$dC_{ND}(t)/dt = K_1C_P(t) - (k_2 + k_3)C_{ND}(t) + k_4C_S(t),$$

$$dC_S(t)/dt = k_3C_{ND}(t) - k_4C_S(t), \text{ and}$$

$$C_T(t) = C_{ND}(t) + C_S(t).$$

$C_T(t)$ is the total radioactivity concentration in a brain region measured by PET.

Calculation of ^{18}F-FE-SPA-RQ Binding Potential (BP_{ND})

^{18}F-FE-SPA-RQ binding was quantified by the indirect kinetic, simplified reference tissue model (SRTM), and ratio methods. In these methods, ^{18}F-FE-SPA-RQ bindings were expressed as BP_{ND} relative to nondisplaceable bindings (*27*). We used the cerebellum as reference brain region because of its negligible NK_1 receptor

FIGURE 1. Typical summated PET images of ^{18}F-FE-SPA-RQ and T1-weighted MR images. Upper row shows slice of cerebellum, and lower row shows slice of caudate, putamen, and cerebral cortex.

density (*20,22,28*). For these analyses, the software package PMOD (PMOD Technologies) was used.

Indirect Kinetic Method. With the cerebellum as reference region, BP_{ND} can be expressed as:

$$BP_{ND} = V_{T(regions)}/V_{T(cerebellum)} - 1,$$

where $V_{T(regions)}$ is the total distribution volume (= $[K_1/k_2][k_3/k_4 + 1]$) of target regions and $V_{T(cerebellum)}$ is that of the cerebellum. K_1, k_2, k_3, and k_4 values were determined by nonlinear least-squares curve fitting to the regional time–activity curves. In this analysis, blood volume (V_b), which depends on the first-pass extraction fraction of the tracer, was assumed to be 0.04 mL/mL, with use of the radioactivity of whole blood to diminish the influence of the tracer remaining in the blood. In this study, the indirect kinetic method was used as the gold standard method (*29*).

SRTM Method. Assuming that both target and reference regions have the same level of nondisplaceable binding, the SRTM can be used to describe time–activity data in the target region as follows (*30*):

$$C_T(t) = R_1C_R(t) + (k_2 - R_1k_2/[1+BP_{ND}])C_R(t)* \exp(-k_2t/[1+BP_{ND}]),$$

where R_1 is the ratio of K_1/K_1' (K_1, influx rate constant for the brain region; K_1', influx rate constant for the reference region), $C_R(t)$ is the radioactivity concentration in the reference region (cerebellum), and * denotes the convolution integral. Using this method, 3 parameters (R_1, k_2, and BP_{ND}) were estimated by a nonlinear curve-fitting procedure. Scan data up to 180, 270, and 330 min were used.

Ratio Method. In the ratio method, BP_{ND} can be expressed as:

$$BP_{ND} = AUC_{(regions)}/AUC_{(cerebellum)} - 1,$$

where $AUC_{(regions)}$ is the area under the time–activity curve of target regions and $AUC_{(cerebellum)}$ is the time–activity curve of the cerebellum. The integration intervals of 120–180, 210–270, and 300–330 min were used.

RESULTS

Typical summated PET images of 4 time periods and T1-weighted MR images are shown in Figure 1. Typical time–activity curves in the brain showed that regional radioactivity was highest in the putamen and caudate (Fig. 2). The next highest region was the parahippocampus, followed by the cerebral cortices and thalamus. Among cerebral

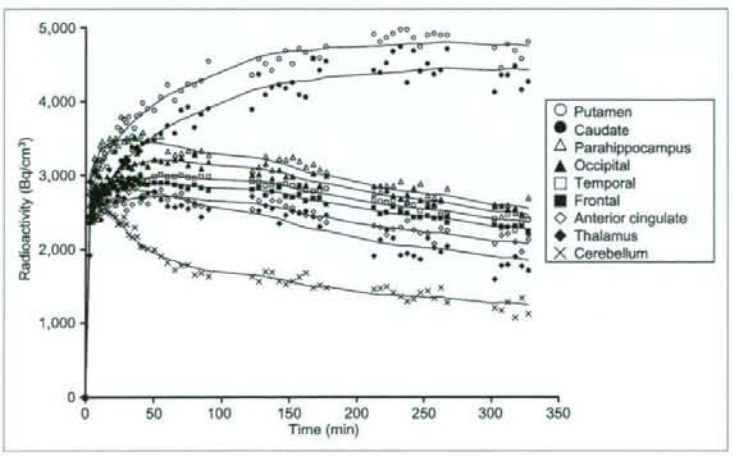

FIGURE 2. Typical time–activity curves of ^{18}F-FE-SPA-RQ in brain. Time–activity curves of all regions could be described by 3CM.

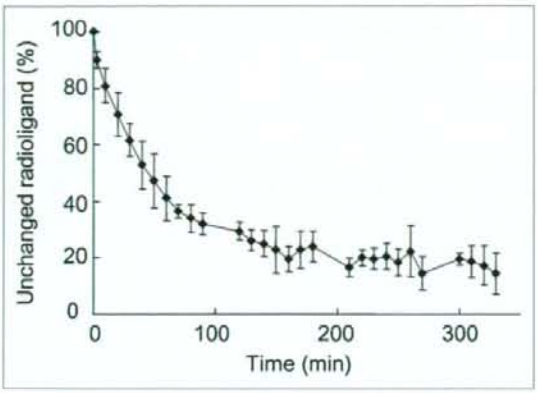

FIGURE 3. Average percentage of unchanged ^{18}F-FE-SPA-RQ in plasma. Bars indicate 1 SD.

cortices, the occipital cortex showed the highest radioactivity. Lowest radioactivity was shown in the cerebellum.

In this study, the fraction of unchanged ^{18}F-FE-SPA-RQ in plasma could not be measured by HPLC analysis in 3 of the 7 subjects because of low radioactivity in blood samples. So, the average of the fractions of unchanged ^{18}F-FE-SPA-RQ in plasma of the other 4 subjects was used for these 3 subjects for the indirect kinetic method. The average percentage fraction of unchanged ^{18}F-FE-SPA-RQ in plasma of the 4 subjects was 90.0% ± 2.9% at 3 min, 80.9% ± 6.1% at 10 min, 32.0% ± 3.9% at 90 min, 23.9% ± 5.3% at 180 min, 14.6% ± 5.9% at 270 min, and 14.4% ± 7.3% at 330 min (Fig. 3).

The rate constants for the 9 regions determined by the kinetic approach using the 3CM with arterial input function are shown in Table 1. For the cerebellum, the 2-compartment model (2CM) without specific binding compartment was also used. Akaike information criteria of the 3CM were significantly lower than those of the 2CM in the cerebellum (290 ± 28 vs. 409 ± 25, $P < 0.0001$; paired t statistics).

The BP_{ND} values of all brain regions calculated by all methods are shown in Table 2. BP_{ND} values by the SRTM method with a scan time of 330 min showed the best correlation with those by the indirect kinetic method (r = 0.98) (Fig. 4A). The SRTM method with scan times of 270 and 180 min and the ratio method with time integration intervals of 300–330, 210–270, and 120–180 min were also in good agreement with the indirect kinetic method in BP_{ND} values (r = 0.94–0.97) (Figs. 4B and 4C; Fig. 5). The BP_{ND} values, except for the caudate and putamen by the SRTM method with a scan time of 180 min and the ratio method with a time integration interval of 120–180 min, were also in good agreement with the indirect kinetic method (SRTM, $r = 0.94$, $y = 0.70x + 0.20$; ratio method, $r = 0.94$, $y = 0.69x + 0.20$).

The BP_{ND} values determined by the kinetic approach ($= k_3/k_4$) were 4.39 ± 3.93 and 5.94 ± 3.44 in the caudate and putamen. Those in the other regions were much smaller and varied widely.

DISCUSSION

After the intravenous injection of ^{18}F-FE-SPA-RQ, radioactivity was highest in the caudate and putamen and lowest in the cerebellum. BP_{ND} values in the caudate and putamen by the indirect kinetic method were 3.15 ± 0.36 and 3.11 ± 0.66, respectively, almost the same as in the previous human PET study with ^{18}F-SPA-RQ (3.08 ± 0.48 in the caudate and 3.71 ± 1.00 in the putamen) (*22*). The parahippocampal region and cerebral cortices showed moderate uptake, and the occipital cortex showed the highest uptake among the cerebral cortices. The thalamus showed relatively low uptake. The uptake shown in these regions was almost the same order of progression as the uptake in previous human PET studies with ^{18}F-SPA-RQ and autoradiographic studies of the human postmortem brain

TABLE 1
Rate Constants for Each Brain Region Determined by Kinetic Approach Using 3CM with Arterial Input Function

Region	Rate constant				Total distribution volume
	K_1 (mL/mL/min)	k_2 (min^{-1})	k_3 (min^{-1})	k_4 (min^{-1})	
Putamen	0.111 ± 0.019	0.036 ± 0.016	0.081 ± 0.040	0.014 ± 0.003	21.3 ± 3.4
Caudate	0.088 ± 0.018	0.023 ± 0.018	0.061 ± 0.067	0.011 ± 0.005	21.5 ± 1.7
Parahippocampus	0.140 ± 0.023	0.033 ± 0.007	0.027 ± 0.020	0.015 ± 0.006	11.3 ± 1.4
Occipital lobe	0.127 ± 0.017	0.065 ± 0.038	0.089 ± 0.057	0.021 ± 0.007	10.0 ± 1.1
Temporal lobe	0.106 ± 0.050	0.050 ± 0.025	0.067 ± 0.038	0.020 ± 0.003	9.5 ± 0.9
Frontal lobe	0.108 ± 0.011	0.041 ± 0.011	0.052 ± 0.023	0.021 ± 0.002	9.1 ± 0.9
Anterior cingulate cortex	0.115 ± 0.014	0.064 ± 0.018	0.072 ± 0.027	0.019 ± 0.005	8.8 ± 0.9
Thalamus	0.112 ± 0.019	0.043 ± 0.018	0.038 ± 0.026	0.019 ± 0.003	7.6 ± 0.9
Cerebellum					
3CM	0.115 ± 0.017	0.051 ± 0.015	0.017 ± 0.008	0.013 ± 0.003	5.2 ± 0.4
2CM	0.089 ± 0.014	0.019 ± 0.002			4.6 ± 0.3

Values are mean ± SD. For cerebellum, both 2CM and 3CM were applied.

TABLE 2
BP_{ND} Values for Each Brain Region with All Methods

Region	Method						
		SRTM (min)			Ratio (min)		
	Indirect kinetic	330	270	180	300–330	210–270	120–180
Putamen	3.11 ± 0.66	2.43 ± 0.33	2.33 ± 0.32	2.20 ± 0.27	2.62 ± 0.40	2.25 ± 0.28	1.81 ± 0.19
Caudate	3.15 ± 0.36	2.14 ± 0.24	2.02 ± 0.22	1.91 ± 0.20	2.31 ± 0.40	1.98 ± 0.26	1.57 ± 0.17
Parahippocampus	1.17 ± 0.25	1.04 ± 0.16	1.02 ± 0.12	1.01 ± 0.12	1.11 ± 0.22	1.05 ± 0.16	1.03 ± 0.20
Occipital lobe	0.94 ± 0.23	0.88 ± 0.14	0.92 ± 0.07	0.90 ± 0.13	0.97 ± 0.16	0.94 ± 0.16	0.95 ± 0.17
Temporal lobe	0.82 ± 0.15	0.77 ± 0.11	0.79 ± 0.08	0.78 ± 0.11	0.85 ± 0.15	0.83 ± 0.15	0.79 ± 0.15
Frontal lobe	0.76 ± 0.15	0.72 ± 0.12	0.74 ± 0.07	0.73 ± 0.11	0.79 ± 0.17	0.76 ± 0.15	0.75 ± 0.15
Anterior cingulate cortex	0.69 ± 0.16	0.66 ± 0.15	0.67 ± 0.13	0.71 ± 0.17	0.70 ± 0.16	0.69 ± 0.13	0.67 ± 0.13
Thalamus	0.46 ± 0.14	0.46 ± 0.13	0.51 ± 0.10	0.49 ± 0.14	0.45 ± 0.12	0.45 ± 0.13	0.49 ± 0.16

Values are mean ± SD.

(*20,22,28*). In a previous autoradiographic study using ^{3}H-GR205171, the maximum number of binding sites for NK_1 receptor in the striatum was 6 times as much as in the cortex (*31*), a result in accordance with the BP_{ND} values in these regions in the present study.

In this study, the indirect kinetic method with arterial blood sampling was used as the gold standard method, because BP_{ND} determined by the kinetic approach as k_3/k_4 showed wide variation. The BP_{ND} values in all brain regions determined by the SRTM method (with scan times of 330, 270, and 180 min) and by the ratio method (with time integration intervals of 300–330, 210–270, and 120–180 min) were in good agreement with those determined by the indirect kinetic method. Although good correlations were observed in BP_{ND} values among the methods, BP_{ND} was underestimated in the caudate and putamen using the

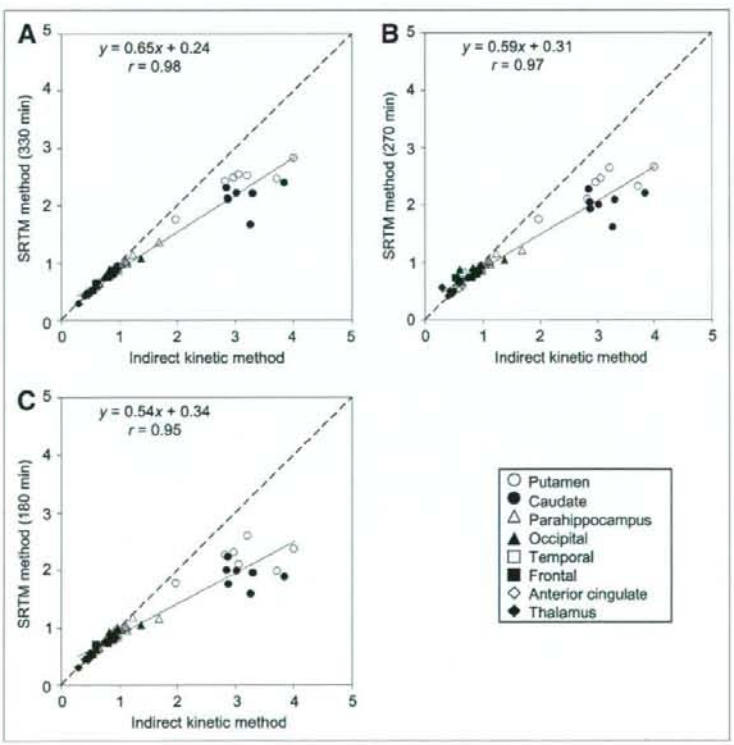

FIGURE 4. Correlation among BP_{ND} values in all brain regions estimated by indirect kinetic and SRTM methods, with scan times of 330 (A), 270 (B), and 180 (C) min.

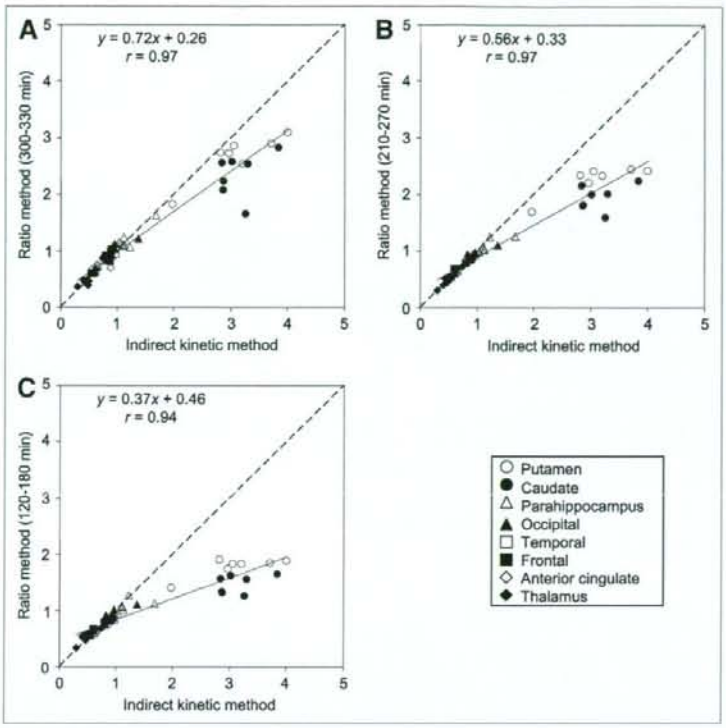

FIGURE 5. Correlation among BP_{ND} values in all brain regions estimated by indirect kinetic and ratio methods, with time integration intervals of 300–330 (A), 210–270 (B), and 120–180 (C) min.

SRTM and ratio methods. The underestimations of BP_{ND} were 32% and 34% in the caudate and 22% and 16% in the putamen for the SRTM method (with a scan time of 330 min) and the ratio method (with a time integration interval of 300–330 min), respectively. More underestimation was observed in the caudate and putamen with the shorter scan time in the SRTM method and with the earlier time integration interval in the ratio method. The reason might be that striatal radioactivity in some subjects did not reach a peak by 330 min. However, the BP_{ND} values of the other regions calculated by the SRTM method (with a scan time of 180 min) and the ratio method (with a time integration interval of 120–180 min) were not greatly underestimated, indicating that the scan time can be shortened to 180 min. Although the indirect kinetic method was considered as the gold standard method, it required a long PET time and arterial blood sampling, an invasive procedure sometimes difficult for patients with psychiatric disorders. The ratio method, which does not require a long PET scanning time and arterial blood sampling, would surely be preferable for clinical investigations. The ratio method, with a time integration interval of 300–330 min, seemed most suitable because the correlation coefficient with the indirect kinetic method was highest and the slope of the regression line was nearest to 1.

The time–activity curves in the cerebellum were well described by the 3CM rather than the 2CM. Similar results were reported for several PET radioligands, with the kinetics in the reference region also being evaluated using the 3CM (*29,32,33*). The results could be explained if the cerebellum would contain specific bindings for NK_1 receptors. However, previous autoradiographic studies showed that the density of NK_1 receptors in the cerebellum was low (*22*), and a previous PET study with ^{18}F-SPA-RQ showed that there was no change in the cerebellar signal before and after high blocking doses of the NK_1 receptor antagonist aprepitant (*20*). Another possible explanation for the results was that the compartments of free and nonspecific binding might have been separated by the kinetic analysis. In addition, ^{18}F-FE-SPA-RQ showed defluorination during the later scans, and bone uptake of ^{18}F might influence the radioactivity in the cerebral cortex and cerebellum adjacent to the skull (although ^{18}F-FE-SPA-RQ showed reduced radioactive accumulation in bone, compared with ^{18}F-SPA-RQ (*23*)).

CONCLUSION

^{18}F-FE-SPA-RQ is a suitable radioligand for PET measurement of NK_1 receptors in the human brain. The 3CM could well describe the brain kinetics of ^{18}F-FE-SPA-RQ. Because the ratio method does not require long scanning times and arterial blood sampling, this method would be useful for clinical research on psychiatric disorders.

ACKNOWLEDGMENTS

We thank Dr. Fumitoshi Kodaka, Dr. Tatsui Otsuka, Katsuyuki Tanimoto, Takahiro Shiraishi, and Akira Ando for their assistance in performing the PET experiments at the National Institute of Radiological Sciences. We also thank Yoshiko Fukushima of the National Institute of Radiological Sciences for her help as clinical research coordinator. This study was supported by a consignment expense for the Molecular Imaging Program on Research Base for PET Diagnosis from the Ministry of Education, Culture, Sports, Science and Technology (MEXT), Japanese Government.

REFERENCES

1. Baker KG, Halliday GM, Hornung JP, Geffen LB, Cotton RG, Tork I. Distribution, morphology and number of monoamine-synthesizing and substance P-containing neurons in the human dorsal raphe nucleus. *Neuroscience.* 1991; 42:757–775.
2. Nicholas AP, Pieribone VA, Arvidsson U, Hokfelt T. Serotonin-, substance P- and glutamate/aspartate-like immunoreactivities in medullo-spinal pathways of rat and primate. *Neuroscience.* 1992;48:545–559.
3. Sergeyev V, Hokfelt T, Hurd Y. Serotonin and substance P co-exist in dorsal raphe neurons of the human brain. *Neuroreport.* 1999;10:3967–3970.
4. Vincent SR, Satoh K, Armstrong DM, Panula P, Vale W, Fibiger HC. Neuropeptides and NADPH-diaphorase activity in the ascending cholinergic reticular system of the rat. *Neuroscience.* 1986;17:167–182.
5. Masu Y, Nakayama K, Tamaki H, Harada Y, Kuno M, Nakanishi S. cDNA cloning of bovine substance-K receptor through oocyte expression system. *Nature.* 1987;329:836–838.
6. Nakanishi S. Mammalian tachykinin receptors. *Annu Rev Neurosci.* 1991; 14:123–136.
7. Ding YQ, Shigemoto R, Takada M, Ohishi H, Nakanishi S, Mizuno N. Localization of the neuromedin K receptor (NK_3) in the central nervous system of the rat. *J Comp Neurol.* 1996;364:290–310.
8. Nakaya Y, Kaneko T, Shigemoto R, Nakanishi S, Mizuno N. Immunohistochemical localization of substance P receptor in the central nervous system of the adult rat. *J Comp Neurol.* 1994;347:249–274.
9. Snider WD, McMahon SB. Tackling pain at the source: new ideas about nociceptors. *Neuron.* 1998;20:629–632.
10. Sanger GJ. Neurokinin NK_1 and NK_3 receptors as targets for drugs to treat gastrointestinal motility disorders and pain. *Br J Pharmacol.* 2004;141:1303–1312.
11. Kincy-Cain T, Bost KL. Increased susceptibility of mice to Salmonella infection following in vivo treatment with the substance P antagonist, spantide II. *J Immunol.* 1996;157:255–264.
12. Metwali A, Blum AM, Elliott DE, Setiawan T, Weinstock JV. Cutting edge: hemokinin has substance P-like function and expression in inflammation. *J Immunol.* 2004;172:6528–6532.
13. Hesketh PJ, Van Belle S, Aapro M, et al. Differential involvement of neurotransmitters through the time course of cisplatin-induced emesis as revealed by therapy with specific receptor antagonists. *Eur J Cancer.* 2003; 39:1074–1080.
14. Hesketh PJ, Grunberg SM, Gralla RJ, et al. The oral neurokinin-1 antagonist aprepitant for the prevention of chemotherapy-induced nausea and vomiting: a multinational, randomized, double-blind, placebo-controlled trial in patients receiving high-dose cisplatin—the Aprepitant Protocol 052 Study Group. *J Clin Oncol.* 2003;21:4112–4119.
15. de Wit R, Herrstedt J, Rapoport B, et al. Addition of the oral NK1 antagonist aprepitant to standard antiemetics provides protection against nausea and vomiting during multiple cycles of cisplatin-based chemotherapy. *J Clin Oncol.* 2003;21:4105–4111.
16. Kramer MS, Cutler N, Feighner J, et al. Distinct mechanism for antidepressant activity by blockade of central substance P receptors. *Science.* 1998;281:1640–1645.
17. Kramer MS, Winokur A, Kelsey J, et al. Demonstration of the efficacy and safety of a novel substance P (NK_1) receptor antagonist in major depression. *Neuropsychopharmacology.* 2004;29:385–392.
18. Keller M, Montgomery S, Ball W, et al. Lack of efficacy of the substance p (neurokinin1 receptor) antagonist aprepitant in the treatment of major depressive disorder. *Biol Psychiatry.* 2006;59:216–223.
19. Solin O, Eskola O, Hamill TG, et al. Synthesis and characterization of a potent, selective, radiolabeled substance-P antagonist for NK_1 receptor quantitation: ([^{18}F]SPA-RQ). *Mol Imaging Biol.* 2004;6:373–384.
20. Bergstrom M, Hargreaves RJ, Burns HD, et al. Human positron emission tomography studies of brain neurokinin 1 receptor occupancy by aprepitant. *Biol Psychiatry.* 2004;55:1007–1012.
21. Hargreaves R. Imaging substance P receptors (NK_1) in the living human brain using positron emission tomography. *J Clin Psychiatry.* 2002;63(suppl 11):S18–S24.
22. Hietala J, Nyman MJ, Eskola O, et al. Visualization and quantification of neurokinin-1 (NK_1) receptors in the human brain. *Mol Imaging Biol.* 2005; 7:262–272.
23. Hamill T, Ryan C, Krause S, et al. The synthesis and in vivo characterization of [^{18}F]FESPARQ, a neurokinin-1 (NK_1) receptor PET ligand [abstract]. *J Labelled Comp Radiopharm.* 2003;46(suppl 1):S35.
24. Haneda E, Higuchi M, Maeda J, et al. In vivo mapping of substance P receptors in brains of laboratory animals by high-resolution imaging systems. *Synapse.* 2007;61:205–215.
25. Zhang MR, Maeda J, Furutsuka K, et al. [^{18}F]FMDAA1106 and [^{18}F]FE-DAA1106: two positron-emitter labeled ligands for peripheral benzodiazepine receptor (PBR). *Bioorg Med Chem Lett.* 2003;13:201–204.
26. Ito H, Takahashi H, Arakawa R, Takano H, Suhara T. Normal database of dopaminergic neurotransmission system in human brain measured by positron emission tomography. *Neuroimage.* 2008;39:555–565.
27. Innis RB, Cunningham VJ, Delforge J, et al. Consensus nomenclature for in vivo imaging of reversibly binding radioligands. *J Cereb Blood Flow Metab.* 2007;27:1533–1539.
28. Caberlotto L, Hurd YL, Murdock P, et al. Neurokinin 1 receptor and relative abundance of the short and long isoforms in the human brain. *Eur J Neurosci.* 2003;17:1736–1746.
29. Ito H, Sudo Y, Suhara T, Okubo Y, Halldin C, Farde L. Error analysis for quantification of [^{11}C]FLB 457 binding to extrastriatal D_2 dopamine receptors in the human brain. *Neuroimage.* 2001;13:531–539.
30. Lammertsma AA, Hume SP. Simplified reference tissue model for PET receptor studies. *Neuroimage.* 1996;4:153–158.
31. Griffante C, Carletti R, Andreetta F, Corsi M. [^{3}H]GR205171 displays similar NK_1 receptor binding profile in gerbil and human brain. *Br J Pharmacol.* 2006; 148:39–45.
32. Farde L, Ito H, Swahn CG, Pike VW, Halldin C. Quantitative analyses of carbonyl-carbon-11-WAY-100635 binding to central 5-hydroxytryptamine-1A receptors in man. *J Nucl Med.* 1998;39:1965–1971.
33. Lundberg J, Odano I, Olsson H, Halldin C, Farde L. Quantification of ^{11}C-MADAM binding to the serotonin transporter in the human brain. *J Nucl Med.* 2005;46:1505–1515.

Quantitative Analysis of Norepinephrine Transporter in the Human Brain Using PET with (S,S)-^{18}F-FMeNER-D_2

Ryosuke Arakawa[1,2], Masaki Okumura[1,2], Hiroshi Ito[1], Chie Seki[1], Hidehiko Takahashi[1], Harumasa Takano[1], Ryuji Nakao[3], Kazutoshi Suzuki[3], Yoshiro Okubo[2], Christer Halldin[4], and Tetsuya Suhara[1]

[1]Molecular Neuroimaging Group, Molecular Imaging Center, National Institute of Radiological Sciences, Chiba, Japan; [2]Department of Neuropsychiatry, Nippon Medical School, Tokyo, Japan; [3]Molecular Probe Group, Molecular Imaging Center, National Institute of Radiological Sciences, Chiba, Japan; and [4]Psychiatry Section, Department of Clinical Neuroscience, Karolinska Institutet, Karolinska Hospital, Stockholm, Sweden

(S,S)-^{18}F-FMeNER-D_2 was recently developed as a radioligand for the measurement of norepinephrine transporter imaging with PET. In this study, a norepinephrine transporter was visualized in the human brain using this radioligand with PET and quantified by several methods. **Methods:** PET scans were performed on 10 healthy men after intravenous injection of (S,S)-^{18}F-FMeNER-D_2. Binding potential relative to nondisplaceable binding (BP_{ND}) was quantified by the indirect kinetic, simplified reference-tissue model (SRTM), multilinear reference-tissue model (MRTM), and ratio methods. The indirect kinetic method was used as the gold standard and was compared with the SRTM method with scan times of 240 and 180 min, the MRTM method with a scan time of 240 min, and the ratio method with a time integration interval of 120–180 min. The caudate was used as reference brain region. **Results:** Regional radioactivity was highest in the thalamus and lowest in the caudate during PET scanning. BP_{ND} values by the indirect kinetic method were 0.54 ± 0.19 and 0.35 ± 0.25 in the thalamus and locus coeruleus, respectively. BP_{ND} values found by the SRTM, MRTM, and ratio methods agreed with the values demonstrated by the indirect kinetic method (r = 0.81–0.92). **Conclusion:** The regional distribution of (S,S)-^{18}F-FMeNER-D_2 in our study agreed with that demonstrated by previous PET and postmortem studies of norepinephrine transporter in the human brain. The ratio method with a time integration interval of 120–180 min will be useful for clinical research of psychiatric disorders for estimation of norepinephrine transporter occupancy by antidepressants without requiring arterial blood sampling and dynamic PET.

Key Words: norepinephrine transporter; (S,S)-^{18}F-FMeNER-D_2; positron emission tomography; human brain; thalamus

J Nucl Med 2008; 49:1270–1276
DOI: 10.2967/jnumed.108.051292

Norepinephrine, one of the monoamine neurotransmitters in the central nervous system, has been reported to be related to several functions such as memory, cognition, consciousness, and emotion and to play important roles in psychiatric disorders (*1–4*). Norepinephrine transporter is responsible for the reuptake of norepinephrine into presynaptic nerves. Norepinephrine reuptake inhibitors are used for the treatment of depression and attention deficit hyperactivity disorder (ADHD) (*4–7*). Thus, changes in norepinephrine transporter functions in several psychiatric disorders can be expected, but in vivo estimation has not been performed because of a lack of suitable radioligands for norepinephrine transporters.

(S,S)-^{18}F-FMeNER-D_2 has recently been developed as a radioligand for the measurement of norepinephrine transporter for PET (*8*). (S,S)-^{18}F-FMeNER-D_2 is a reboxetine analog and has high affinity for norepinephrine transporter and high selectivity from other monoamine transporters. Tracer distribution and dosimetry of (S,S)-^{18}F-FMeNER-D_2 were reported in monkey (*8,9*) and human studies (*10,11*). Another monkey study showed that (S,S)-^{18}F-FMeNER-D_2 binding decreased by the administration of atomoxetine, a selective norepinephrine reuptake inhibitor (*12*). However, quantitative analyses of (S,S)-^{18}F-FMeNER-D_2 bindings using an arterial input function have not yet, to our knowledge, been performed.

In this study, we aimed to quantify the norepinephrine transporter bindings in the human brain using (S,S)-^{18}F-FMeNER-D_2 with arterial blood sampling and also to validate noninvasive methods for quantification without arterial blood sampling.

MATERIALS AND METHODS

Subjects

Ten healthy men (age range, 21–26 y; mean ± SD, 22.7 ± 1.6 y) participated in this study. All subjects were free of any somatic, neurologic, or psychiatric disorders, and they had no

Received Jan. 30, 2008; revision accepted May 2, 2008.
For correspondence or reprints contact: Hiroshi Ito, Molecular Neuroimaging Group, Molecular Imaging Center, National Institute of Radiological Sciences, 4-9-1, Anagawa, Inage-ku, Chiba, 263-8555, Japan.
E-mail: hito@nirs.go.jp

history of current or previous drug abuse. Written informed consent was obtained from all subjects following a complete description of this study. The study was approved by the Ethics and Radiation Safety Committee of the National Institute of Radiologic Sciences, Chiba, Japan.

PET Procedure

(S,S)-^{18}F-FMeNER-D_2 was synthesized by fluoromethylation of nor-ethyl-reboxetine with ^{18}F-bromofluoromethane-d_2 as previously described (*8*). A PET scanner system (ECAT EXACT HR+; CTI-Siemens) was used for all subjects, with a head holder used to minimize head movement. A transmission scan for attenuation correction was performed using a ^{68}Ge–^{68}Ga source. Dynamic PET scans were performed after a 1-min intravenous slow bolus injection of 353.4–382.7 MBq (mean ± SD, 368.1 ± 9.1 MBq) of (S,S)-^{18}F-FMeNER-D_2. The specific radioactivity of (S,S)-^{18}F-FMeNER-D_2 was 144.8–390.2 GBq/μmol (312.8 ± 76.2 GBq/μmol). Brain radioactivities were measured from 0 to 90 min (1 min × 10, 2 min × 15, and 5 min × 10), from 120 to 180 min (10 min × 6), and from 210 to 240 min (10 min × 3). MR images of the brain were acquired with a 1.5-T MRI scanner (Gyroscan NT; Philips). T1-weighted images were obtained at 1-mm slices.

Arterial Blood Sampling and Metabolite Analysis

To obtain the arterial input function, arterial blood samples were taken manually 42 times during the PET scan. Each blood sample was centrifuged to obtain plasma and blood cell fractions, and the concentrations of radioactivity in whole blood and in plasma were measured.

The percentage of unchanged (S,S)-^{18}F-FMeNER-D_2 in plasma was determined by high-performance liquid chromatography in 22 of the blood samples. Acetonitrile was added to each plasma sample, and samples were centrifuged. The supernatant was subjected to high-performance liquid chromatography radiodetection analysis (column: XBridge Prep C18, mobile phase, 90% acetonitrile/50 mM ammonium acetate = 48/52; Waters). Plasma input function was defined as radioactivity of plasma multiplied by the percentage of unchanged radioligand.

Regions of Interest

All MR images were coregistered to the PET images using a statistical parametric mapping system (SPM2; The Wellcome Trust Centre for Neuroimaging, University College London). Regions of interest were drawn manually on summed PET images, with reference to coregistered MR images, and were defined for the thalamus, locus coeruleus, hippocampus, anterior cingulate gyrus, and caudate head. Regional radioactivity was calculated for each frame, corrected for decay, and plotted versus time.

Kinetic Model of ^{18}F-FMeNER-D_2

To describe the kinetics of (S,S)-^{18}F-FMeNER-D_2 in the brain, the 3-compartment model with 4 first-order rate constants was used. The 3 compartments were defined as follows: C_P was the radioactivity concentration of unchanged radioligand in plasma (arterial input function), C_{ND} was the radioactivity concentration of nondisplaceable radioligand in the brain, including nonspecifically bound and free radioligand, and C_S was the radioactivity concentration of radioligand specifically bound to transporters. The rate constants K_1 and k_2 represent the influx and efflux rates, respectively, for radioligand diffusion through the blood–brain barrier, and the rate constants k_3 and k_4 are the radioligand transfers between the compartments for nondisplaceable and specifically bound radioligand, respectively. This model can be described by the following equations:

$$\frac{dC_{ND}(t)}{dt} = K_1C_P(t) - (k_2+k_3)C_{ND}(t) + k_4C_S(t),$$

$$\frac{dC_S(t)}{dt} = k_3C_{ND}(t) - k_4C_S(t), \text{ and}$$

$$C_T(t) = C_{ND}(t)+C_S(t).$$

$C_T(t)$ is the total radioactivity concentration in any brain region measured by PET.

Calculation of (S,S)-^{18}F-FMeNER-D_2 Binding Potential

(S,S)-^{18}F-FMeNER-D_2 binding was quantified by the indirect kinetic, simplified reference-tissue model (SRTM), multilinear reference-tissue model (MRTM), and ratio methods. In these methods, (S,S)-^{18}F-FMeNER-D_2 bindings were expressed as binding potentials relative to nondisplaceable binding (BP_{ND}) (*13*). We used the caudate as the reference brain region because of its

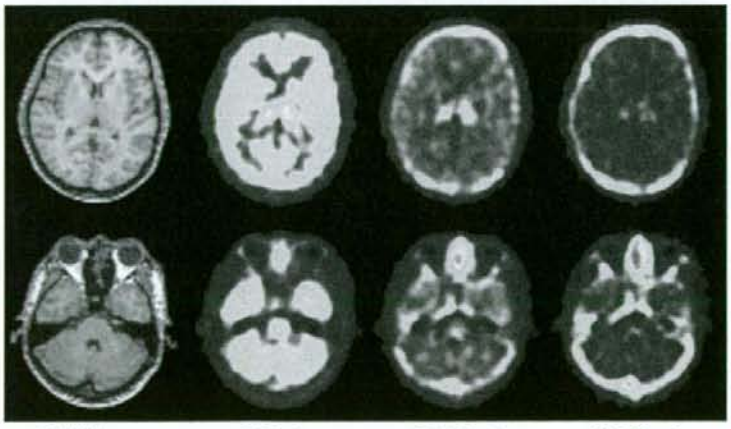

FIGURE 1. Typical summed PET images of (S,S)-^{18}F-FMeNER-D_2 and T1-weighted MR images. Upper panel shows slice of caudate and thalamus, and lower panel shows slice of locus coeruleus.

negligible norepinephrine transporter density (*14–16*). Software (PMOD; PMOD Technologies) was used for these analyses.

Indirect Kinetic Method

With the caudate as reference region, BP_{ND} can be expressed as:

$$BP_{ND} = \frac{V_{T(regions)}}{V_{T(caudate)}} - 1,$$

where $V_{T(regions)}$ is the total distribution volume (= $[K_1/k_2][k_3/k_4 + 1]$) of target regions and $V_{T(caudate)}$ is the total distribution volume of the caudate. The K_1, k_2, k_3, and k_4 values were determined by nonlinear least-squares curve fitting to the regional time–activity curves. In this analysis, blood volume (V_b), which depends on the first-pass extraction fraction of the tracer, was also estimated using the radioactivity of whole blood to diminish the influence of the tracer remaining in the blood. In this study, the indirect kinetic method was used as the standard method (*17*).

SRTM Method

Assuming that both target and reference regions have the same level of nondisplaceable binding, the SRTM method can be used to describe time–activity data in the target region as follows (*18*):

$$C_T(t) = R_1 C_R(t) + \left(k_2 - R_1 \frac{k_2}{1+BP_{ND}}\right) C_R(t) \otimes \exp\left(\frac{-k_2}{1+BP_{ND}} t\right),$$

where R_1 is the ratio of K_1/K_1' (K_1, influx rate constant for the brain region; K_1', influx rate constant for the reference region), $C_R(t)$ is the radioactivity concentration in the reference region (caudate), and $\otimes$ denotes the convolution integral. Using this model, 3 parameters (R_1, k_2, and BP_{ND}) were estimated by a nonlinear curve-fitting procedure. Scan data up to 180 or 240 min were used.

MRTM Method

The MRTM method is one of the variations of the graphical approaches (*19*). After a certain equilibrium time (t*), the following multilinear regression is obtained:

$$C_T(T) = -\frac{V_{T(regions)}}{V_{T(caudate)}} \int_0^T C_R(t)dt + \frac{1}{b} \int_0^T C_T(t)dt - \frac{V_{T(regions)}}{V_{T(caudate)} k_2' b} C_R(T),$$

where k_2' is the efflux rate constant for the reference region. In this analysis, t* was determined so that the maximum error from the regression within the linear segment would be 10% for each time–activity curve. BP_{ND} for the MRTM method was calculated using the same equation as described previously for the indirect kinetic method (= $V_{T(regions)}/V_{T(caudate)} - 1$). Scan data up to 240 min were used.

Ratio Method

In the ratio method, BP_{ND} can be expressed as:

$$BP_{ND} = \frac{AUC_{(regions)}}{AUC_{(caudate)}} - 1,$$

where $AUC_{(regions)}$ is the area under the time–activity curve of the target regions and $AUC_{(caudate)}$ is the area under the time–activity curve of the caudate. The integration interval of 120–180 min was used in this method.

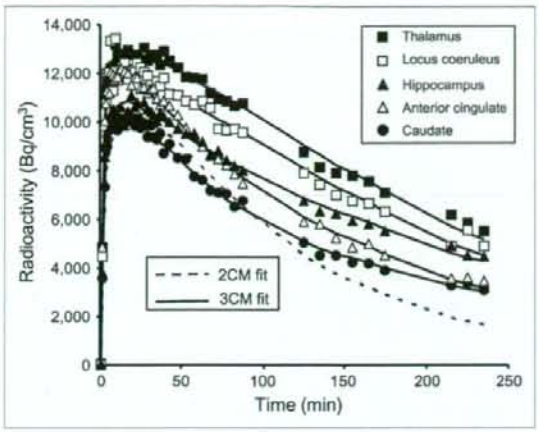

FIGURE 2. Typical time–activity curves of (S,S)-^{18}F-FMeNER-D_2 in brain. Time–activity curves of all regions could be described by 3-compartment model (3CM). Time–activity curve of caudate could also be described by 2-compartment model (2CM).

Simulation Study

A simulation study was performed to estimate errors in BP_{ND} calculated by the SRTM and ratio methods. Tissue time–activity curves for the thalamus were generated using the 3-compartment model. The rate constant values K_1, k_2, and k_4 of the thalamus were assumed to be 0.157, 0.037, and 0.016, respectively. The value of k_3 ranged from 0.019 to 0.039 in 6 steps. Tissue time–activity curves for the caudate were also generated using the 3-compartment model, assuming that the rate constant values K_1, k_2, k_3, and k_4 were 0.124, 0.032, 0.010, and 0.010, respectively. These assumed values were taken from the results obtained by the kinetic approach. The average of arterial input function for all

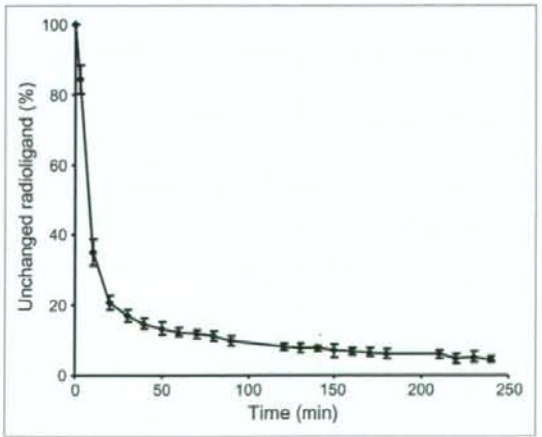

FIGURE 3. Average percentage of unchanged (S,S)-^{18}F-FMeNER-D_2 in plasma. Bars indicate 1 SD.

TABLE 1
Data for Each Brain Region Determined by Kinetic Approach Using 3-Compartment Model with Arterial Input Function

Region	V_b	Rate constant				V_{ND}	V_T
		K_1 (mL/mL/min)	k_2 (min^{-1})	k_3 (min^{-1})	k_4 (min^{-1})		
Thalamus	0.045 ± 0.016	0.157 ± 0.025	0.037 ± 0.005	0.027 ± 0.007	0.016 ± 0.002	4.36 ± 0.90	11.45 ± 2.29
Locus coeruleus	0.032 ± 0.008	0.154 ± 0.026	0.040 ± 0.009	0.020 ± 0.008	0.013 ± 0.004	4.06 ± 1.01	9.89 ± 1.78
Hippocampus	0.038 ± 0.010	0.119 ± 0.013	0.035 ± 0.011	0.022 ± 0.016	0.015 ± 0.005	3.73 ± 0.83	8.48 ± 1.14
Anterior cingulate	0.053 ± 0.011	0.144 ± 0.019	0.032 ± 0.005	0.010 ± 0.005	0.012 ± 0.004	4.61 ± 1.04	8.33 ± 1.70
Caudate (3-compartment model)	0.031 ± 0.008	0.124 ± 0.018	0.032 ± 0.005	0.010 ± 0.005	0.010 ± 0.004	3.92 ± 0.80	7.51 ± 1.51
Caudate (2-compartment model)	0.045 ± 0.010	0.109 ± 0.017	0.019 ± 0.001			5.77 ± 0.98	

Values are mean ± SD. V_{ND} is defined as K_1/k_2 and V_T as $(K_1/k_2)(k_3/k_4 + 1)$.

subjects was used to generate the time–activity curves. With these generated time–activity curves, BP_{ND} values were calculated by the SRTM (scan time of 240 min), MRTM, and ratio methods. The calculated BP_{ND} values for the simulation study were compared with those calculated by the indirect kinetic method.

RESULTS

Typical summed PET images of 3 time periods and T1-weighted MR images are shown in Figure 1. Typical time–activity curves in the brain showed that regional radioactivity was highest in the thalamus and lowest in the caudate (Fig. 2). Time–activity curves for all regions could be described by the 3-compartment model. The time–activity curve for the caudate could also be described by the 2-compartment model. The average percentage of unchanged (S,S)-^{18}F-FMeNER-D_2 in plasma was 84.4% ± 3.9% at 3 min, 35.1% ± 3.7% at 10 min, 10.0% ± 1.4% at 90 min, 6.1% ± 1.3% at 180 min, and 4.5% ± 0.9% at 240 min (Fig. 3).

The blood volume, rate constants, nondisplaceable distribution volume (V_{ND}), and total distribution volume (V_T) for each brain region determined by the kinetic approach using the 3-compartment model with arterial input function are shown in Table 1. For the caudate, the 2-compartment model without a specific binding compartment was also applied. Akaike information criteria of the 3-compartment model were lower than those of the 2-compartment model (143 ± 16 vs. 227 ± 6, $P < 0.0001$; paired t statistics).

The BP_{ND} values of the thalamus calculated by all methods are shown in Table 2. BP_{ND} values in the thalamus by the MRTM method showed the best correlation with those by the indirect kinetic method ($r = 0.92$) (Fig. 4C). The SRTM method with scan times of 180 and 240 min and the ratio method also agreed with the BP_{ND} values by the indirect kinetic method ($r = 0.81$–0.91) (Figs. 4A, 4B, and 4D). However, BP_{ND} values in brain regions other than the thalamus could not be estimated by the SRTM and MRTM methods because of failed curve fitting, showing no convergence. The BP_{ND} values of each brain region by the indirect kinetic and ratio methods are shown in Table 3. The correlation of BP_{ND} values in all target regions between the indirect kinetic and the ratio methods is shown in Figure 5A. The Bland–Altman plot of BP_{ND} values by these 2 methods is shown in Figure 5B.

In the simulation study, estimated BP_{ND} values, compared with assumed BP_{ND} values, by the SRTM (scan time of 240 min), MRTM, and ratio methods were slightly overestimated (Fig. 6).

DISCUSSION

After intravenous injection of (S,S)-^{18}F-FMeNER-D_2, radioactivity was highest in the thalamus and lowest in the caudate. BP_{ND} in the thalamus using the ratio method was 0.67 ± 0.15, almost the same value as found in a previous human PET study (*10*). The locus coeruleus showed relatively high uptake, and the hippocampus and anterior cingulate cortex showed relatively low uptake. This result was in agreement with previous reports that the thalamus and locus coeruleus showed high densities of norepinephrine transporters (*14–16,20*). Previous autoradiographic studies with human postmortem brains reported that norepinephrine transporter density in the locus coeruleus was higher by about 10 times than that in the thalamus (*14,15*). However,

TABLE 2
BP_{ND} Values in Thalamus by All Methods

Method	BP_{ND}
Indirect kinetic	0.54 ± 0.19
SRTM (240 min)	0.61 ± 0.14
SRTM (180 min)	0.64 ± 0.14
MRTM	0.61 ± 0.14
Ratio	0.67 ± 0.15

Values are mean ± SD.

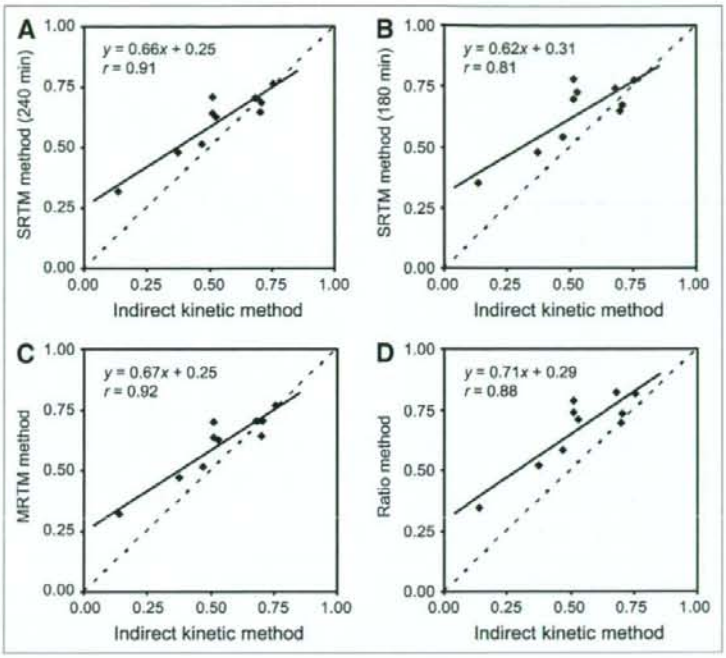

FIGURE 4. Correlation between BP_{ND} values in thalamus estimated by indirect kinetic method and SRTM method with scan time of 240 min (A) or 180 min (B), MRTM method (C), or ratio method (D).

previous and present PET studies reported almost the same values between the locus coeruleus and thalamus (*10,16*). One possible reason for the discrepancy was the partial-volume effect due to the limited spatial resolution of the PET scanner, the locus coeruleus being a very small structure.

In the current study, the indirect kinetic method with arterial blood sampling was used as the standard method (*17*). The BP_{ND} values in the thalamus by the other 3 methods—the SRTM with scan times of 240 and 180 min, MRTM, and ratio methods—were in agreement with those found by the indirect kinetic method. Although the indirect kinetic method was considered the standard method, it required a long PET time as well as arterial blood sampling, an invasive procedure particularly unsuitable for patients with psychiatric disorders. Because the ratio method does not require long PET and arterial blood sampling, this method would be preferable for clinical investigation. The SRTM and MRTM methods can estimate only the thalamus, as curve fitting failed in other brain regions. The MRTM2 method (*19*) may be able to estimate BP_{ND} in regions other than thalamus; however, weighted k_2' value among brain regions could not be calculated in this tracer. The possible reasons of failed curve fitting might be the small differences of time–activity curves between target and reference regions and the noise in time–activity curves. The ratio method could reveal BP_{ND} values in brain regions other than the thalamus. The BP_{ND} values by the ratio method were in agreement with those by the indirect kinetic method for all brain regions (Fig. 5A). Although bias was observed by the ratio method, this bias did not change according to the BP_{ND} values (Fig. 5B). The ratio method could estimate norepinephrine transporter binding in the thalamus and also other brain regions.

The time–activity curves in the caudate were better described by the 3-compartment model than the 2-compartment model. Similar results were reported for several PET radioligands; the kinetics in the reference region were also evaluated using the 3-compartment model (*17,21,22*). The results could be explained if the caudate contained specific binding for norepinephrine transporters. However, previous autoradiographic studies showed that the density of norepinephrine transporters in the caudate was very low (*14–16*). Another possible explanation is that the compartments of free and nonspecific binding could be separated by the kinetic analysis. Moreover, spillover from

TABLE 3
BP_{ND} Values for Each Brain Region by Indirect Kinetic and Ratio Methods

Region	Indirect kinetic method	Ratio method
Thalamus	0.54 ± 0.19	0.67 ± 0.15
Locus coeruleus	0.35 ± 0.25	0.42 ± 0.13
Hippocampus	0.13 ± 0.14	0.23 ± 0.09
Anterior cingulate	0.13 ± 0.16	0.15 ± 0.09

Values are mean ± SD.

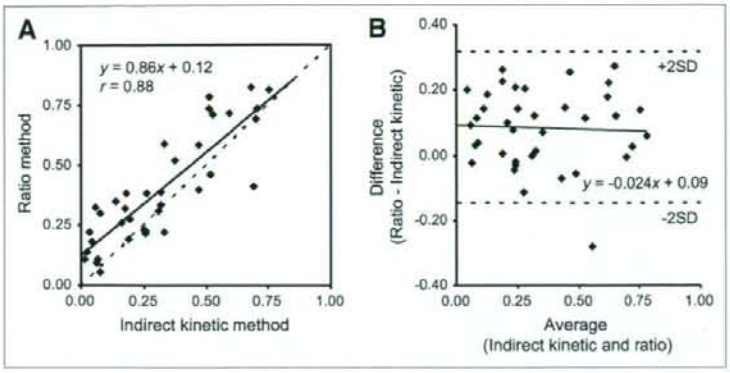

FIGURE 5. Correlation between BP_{ND} values in all target regions estimated by indirect kinetic method and ratio method (A) and Bland–Altman plot (B).

other brain regions to the caudate may affect the results because the caudate is a small structure and is surrounded by regions with specific binding.

In this study, we investigated norepinephrine transporter binding in only limited regions. Other brain regions such as the cerebral cortex and cerebellum are also considered to possess norepinephrine neurons and norepinephrine transporters (*14–16*). However, (S,S)-^{18}F-FMeNER-D_2 showed that defluorination and uptake of ^{18}F in the skull influenced cerebral radioactivity (*8*). Although (S,S)-^{18}F-FMeNER-D_2 had reduced defluorination by the dideuteration, compared with (S,S)-^{18}F-FMeNER, estimation in the cerebral cortex or cerebellum adjacent to the skull was considered difficult.

In this study, occupancy of norepinephrine transporter by antidepressants was not evaluated. Previous animal studies showed dose-dependent norepinephrine transporter occupancy by atomoxetine (*12*). However, a human study using [^{11}C](S,S)-MRB reported no differences in occupancy between different doses of atomoxetine (*16*). Further, occupancy studies in humans to estimate the clinical effects of antidepressants, similar to occupancy studies for dopamine D_2 receptor and serotonin transporters (*23,24*), will be needed.

In the simulation study, BP_{ND} values by the SRTM with a scan time of 240 min, MRTM, and the ratio methods were overestimated, compared with assumed BP_{ND} (Fig. 6). Such overestimation was also observed in measured PET data, especially in regions with low specific binding (Figs. 4A, 4C, and 4D). The degree of overestimation of BP_{ND} was larger in measured data than that in the simulation, especially in regions with low specific binding. Noise in measured data might cause such discrepancy, and therefore further studies using simulated data with added noise may be required. Although linear correlation was observed in BP_{ND} values between the ratio and indirect kinetic methods, this overestimation may cause errors in the calculation of occupancy by antidepressants. When baseline BP_{ND} is 0.6, estimated occupancy by the ratio method is 22%, 43%, and 65%, corresponding to the assumed occupancy of 25%, 50%, and 75%, respectively (Fig. 6). The SRTM and MRTM methods also showed the underestimation of occupancy, 21%, 43%, and 64% by the former and 21%, 42%, and 63% by the latter.

CONCLUSION

(S,S)-^{18}F-FMeNER-D_2 is a suitable radioligand for PET measurement of norepinephrine transporters in the human brain. The 3-compartment model could well describe the brain kinetics of (S,S)-^{18}F-FMeNER-D_2. Because the ratio method does not require long PET imaging times and arterial blood sampling, this method would be useful for clinical research of psychiatric disorders.

ACKNOWLEDGMENTS

We thank Dr. Fumitoshi Kodaka, Dr. Tatsui Otsuka, Katsuyuki Tanimoto, Takahiro Shiraishi, and Akira Ando

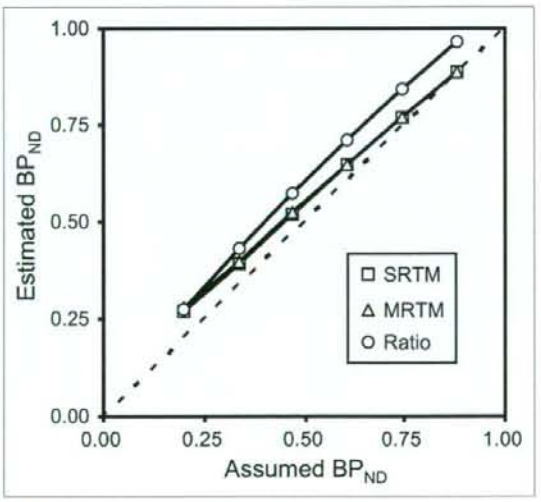

FIGURE 6. Correlations between assumed BP_{ND} values by indirect kinetic method and those by SRTM with scan time of 240 min, MRTM method, or ratio method in simulation studies.

for their assistance in performing the PET experiments at the National Institute of Radiological Sciences. We also thank Yoshiko Fukushima of the National Institute of Radiological Sciences for her help as clinical research coordinator. This study was supported by a consignment expense for the Molecular Imaging Program on Research Base for PET Diagnosis from the Ministry of Education, Culture, Sports, Science and Technology (MEXT), Japanese government, and by a Health and Labor Sciences Research Grant for Research on Psychiatric and Neurological Diseases and Mental Health from the Ministry of Health, Labor and Welfare, Japanese government.

REFERENCES

1. Harmer CJ, Shelley NC, Cowen PJ, Goodwin GM. Increased positive versus negative affective perception and memory in healthy volunteers following selective serotonin and norepinephrine reuptake inhibition. *Am J Psychiatry.* 2004;161:1256–1263.
2. Strange BA, Hurlemann R, Dolan RJ. An emotion-induced retrograde amnesia in humans is amygdala- and beta-adrenergic-dependent. *Proc Natl Acad Sci USA.* 2003;100:13626–13631.
3. Southwick SM, Davis M, Horner B, et al. Relationship of enhanced norepinephrine activity during memory consolidation to enhanced long-term memory in humans. *Am J Psychiatry.* 2002;159:1420–1422.
4. Nutt DJ. The role of dopamine and norepinephrine in depression and antidepressant treatment. *J Clin Psychiatry.* 2006;67(suppl 6):3–8.
5. Cheng JY, Chen RY, Ko JS, Ng EM. Efficacy and safety of atomoxetine for attention-deficit/hyperactivity disorder in children and adolescents: meta-analysis and meta-regression analysis. *Psychopharmacology (Berl).* 2007;194:197–209.
6. Chamberlain SR, Del Campo N, Dowson J, et al. Atomoxetine improved response inhibition in adults with attention deficit/hyperactivity disorder. *Biol Psychiatry.* 2007;62:977–984.
7. Shelton RC. The dual-action hypothesis: does pharmacology matter? *J Clin Psychiatry.* 2004;65(suppl 17):5–10.
8. Schou M, Halldin C, Sovago J, et al. PET evaluation of novel radiofluorinated reboxetine analogs as norepinephrine transporter probes in the monkey brain. *Synapse.* 2004;53:57–67.
9. Seneca N, Andree B, Sjoholm N, et al. Whole-body biodistribution, radiation dosimetry estimates for the PET norepinephrine transporter probe (*S,S*)-[^{18}F]FMeNER-D2 in non-human primates. *Nucl Med Commun.* 2005;26:695–700.
10. Takano A, Gulyas B, Varrone A, et al. Imaging the norepinephrine transporter with positron emission tomography: initial human studies with (*S,S*)-[^{18}F]FMeNER-D_2. *Eur J Nucl Med Mol Imaging.* 2008;35:153–157.
11. Takano A, Halldin C, Varrone A, et al. Biodistribution and radiation dosimetry of the norepinephrine transporter radioligand (*S,S*)-[^{18}F]FMeNER-D_2: a human whole-body PET study. *Eur J Nucl Med Mol Imaging.* 2008;35:630–636.
12. Seneca N, Gulyas B, Varrone A, et al. Atomoxetine occupies the norepinephrine transporter in a dose-dependent fashion: a PET study in nonhuman primate brain using (*S,S*)-[^{18}F]FMeNER-D2. *Psychopharmacology (Berl).* 2006;188:119–127.
13. Innis RB, Cunningham VJ, Delforge J, et al. Consensus nomenclature for in vivo imaging of reversibly binding radioligands. *J Cereb Blood Flow Metab.* 2007;27:1533–1539.
14. Schou M, Halldin C, Pike VW, et al. Post-mortem human brain autoradiography of the norepinephrine transporter using (*S,S*)-[^{18}F]FMeNER-D2. *Eur Neuropsychopharmacol.* 2005;15:517–520.
15. Donnan GA, Kaczmarczyk SJ, Paxinos G, et al. Distribution of catecholamine uptake sites in human brain as determined by quantitative [^{3}H] mazindol autoradiography. *J Comp Neurol.* 1991;304:419–434.
16. Logan J, Wang GJ, Telang F, et al. Imaging the norepinephrine transporter in humans with (*S,S*)-[^{11}C]O-methyl reboxetine and PET: problems and progress. *Nucl Med Biol.* 2007;34:667–679.
17. Ito H, Sudo Y, Suhara T, Okubo Y, Halldin C, Farde L. Error analysis for quantification of [^{11}C]FLB 457 binding to extrastriatal D_2 dopamine receptors in the human brain. *Neuroimage.* 2001;13:531–539.
18. Lammertsma AA, Hume SP. Simplified reference tissue model for PET receptor studies. *Neuroimage.* 1996;4:153–158.
19. Ichise M, Liow JS, Lu JQ, et al. Linearized reference tissue parametric imaging methods: application to [^{11}C]DASB positron emission tomography studies of the serotonin transporter in human brain. *J Cereb Blood Flow Metab.* 2003;23:1096–1112.
20. Ordway GA, Stockmeier CA, Cason GW, Klimek V. Pharmacology and distribution of norepinephrine transporters in the human locus coeruleus and raphe nuclei. *J Neurosci.* 1997;17:1710–1719.
21. Lundberg J, Odano I, Olsson H, Halldin C, Farde L. Quantification of ^{11}C-MADAM binding to the serotonin transporter in the human brain. *J Nucl Med.* 2005;46:1505–1515.
22. Farde L, Ito H, Swahn CG, Pike VW, Halldin C. Quantitative analyses of carbonyl-carbon-11-WAY-100635 binding to central 5-hydroxytryptamine-1A receptors in man. *J Nucl Med.* 1998;39:1965–1971.
23. Takano A, Suzuki K, Kosaka J, et al. A dose-finding study of duloxetine based on serotonin transporter occupancy. *Psychopharmacology (Berl).* 2006;185:395–399.
24. Arakawa R, Ito H, Takano A, et al. Dose-finding study of paliperidone ER based on striatal and extrastriatal dopamine D_2 receptor occupancy in patients with schizophrenia. *Psychopharmacology (Berl).* 2008;197:229–235.

NeuroImage 42 (2008) 1285–1294

Contents lists available at ScienceDirect

NeuroImage

journal homepage: www.elsevier.com/locate/ynimg

Error analysis for PET measurement of dopamine D_2 receptor occupancy by antipsychotics with [^{11}C]raclopride and [^{11}C]FLB 457

Yoko Ikoma [a,b], Hiroshi Ito [a,*], Ryosuke Arakawa [a], Masaki Okumura [a], Chie Seki [a], Miho Shidahara [a], Hidehiko Takahashi [a], Yuichi Kimura [a], Iwao Kanno [a], Tetsuya Suhara [a]

[a] Molecular Imaging Center, National Institute of Radiological Sciences 4-9-1, Anagawa, Inage-ku, Chiba, 263-8555, Japan
[b] Department of Investigative Radiology, National Cardiovascular Center Research Institute, Osaka, Japan

ARTICLE INFO

Article history:
Received 14 February 2008
Revised 14 May 2008
Accepted 31 May 2008
Available online 10 June 2008

Keywords:
Positron emission tomography
Dopamine D_2 receptor
Occupancy
[^{11}C]raclopride
[^{11}C]FLB 457

ABSTRACT

Dopamine D_2 receptor occupancy by antipsychotic drugs has been measured with positron emission tomography (PET) by comparing the binding potential (BP) values before and after drug administration. This occupancy has been found to be related to clinical effects and side effects. In this study, we evaluated the uncertainty of the quantitative analysis for estimating the dopamine D_2 receptor occupancy by antipsychotics in simulation and human studies of [^{11}C]raclopride and for the high affinity ligand [^{11}C]FLB 457. Time–activity curves of [^{11}C]raclopride and [^{11}C]FLB 457 were simulated, and the reliability of BP estimated by a simplified reference tissue model and the calculated occupancy were investigated for various noise levels, BP values, and scan durations. Then, in the human PET study with and without antipsychotics, the uncertainty of BP and occupancy estimates and the scan duration required for a reliable estimation were investigated by a bootstrap approach. Reliable and unbiased estimates of [^{11}C]raclopride BP_{ND} could be obtained with recording as short as 32 min, with the relative standard deviation (SD) of the striatal occupancy remaining less than 10%. Conversely, in [^{11}C]FLB 457 studies, the mean value increased and SD of the temporal cortex and thalamus exceeded 10% when the scan duration was shorter than 60 min. These results demonstrated that dopamine D_2 receptor occupancy by antipsychotics can be estimated precisely with an optimal scan duration with [^{11}C]raclopride and [^{11}C]FLB 457.

Introduction

Neuroreceptor imaging with positron emission tomography (PET) has made it possible to measure dopamine D_2 receptor occupancy by antipsychotic drugs in the living human brain (Farde et al., 1988, 1990). Raclopride has been widely used as a radioligand for PET measurement of striatal dopamine D_2 receptor binding (Farde et al., 1985). Using this competition paradigm, it has been shown that dopamine D_2 receptor occupancy in the striatum measured with [^{11}C] raclopride in antipsychotic drug-treated patients was related to clinical effects including antipsychotic effects and extrapyramidal symptoms (Farde et al., 1992a,b; Farde and Nordstrom, 1993; Nordstrom et al., 1993; Nyberg et al., 1995; Kapur et al., 2000). However, due to its low affinity for dopamine D_2 receptors, [^{11}C]raclopride is not suitable for measuring dopamine D_2 receptor binding in extrastriatal regions with low receptor densities. Extrastriatal regions, in particular cerebral cortices with low density of dopamine D_2 receptors, have been suggested to be the important sites for antipsychotic action, especially for the so-called atypical antipsychotics (Lidow et al., 1998; Pilowsky et al., 1997). [^{11}C] FLB 457, which has a high affinity for dopamine D_2 receptors, was shown to be suitable for the quantification of low-density extrastriatal dopamine receptors using PET (Halldin et al., 1995; Farde et al., 1997; Delforge et al., 1999; Olsson et al., 1999; Suhara et al., 1999), and has been applied for the measurement of receptor occupancy in extrastriatal regions (Farde et al., 1997; Talvik et al., 2001; Agid et al., 2007; Mizrahi et al., 2007). However, because of its slow kinetics, the time point of reaching equilibrium in receptor-rich regions is beyond the end of the data acquisition time, and thus the binding of [^{11}C]FLB 457 cannot be measured in the striatum for the practical data with noise (Olsson and Farde, 2001).

Receptor occupancy can be estimated from reductions in the observed binding potential evoked by competition from antipsychotic medication. Several quantitative methods have been proposed for estimating binding potential, and recently a

* Corresponding author. Fax: +81 43 253 0396.
E-mail address: hito@nirs.go.jp (H. Ito).

1053-8119/$ – see front matter © 2008 Elsevier Inc. All rights reserved.
doi:10.1016/j.neuroimage.2008.05.056

Table 1
Subjects and procedure of [^{11}C]raclopride study

Antipsychotic drug	Number of subjects	Age mean±SD	Dose of antipsychotic [mg]	Scan start time after antipsychotic administration [h]
Risperidon	5	28.6±6.2	2	2
Quetiapin	3	25.0±6.9	400	8
Perospirone	3	28.3±4.0	16	8

simplified reference tissue model (Lammertsma and Hume, 1996) has often been used in [^{11}C]raclopride and [^{11}C]FLB 457 studies, a method employing a reference region with negligible specific binding to avoid arterial blood sampling. Because binding potential varies widely in occupancy studies, accuracy of the measurement of wide range binding potential should be confirmed.

In this study, we evaluated errors in quantitative analysis for estimating dopamine D_2 receptor occupancy by antipsychotics with [^{11}C]raclopride and [^{11}C]FLB 457 in simulation and human studies. The effect of scan duration on the error of estimates was also evaluated.

Materials and methods

Estimation of receptor occupancy

Simplified reference tissue model (SRTM)

This method yields the binding potential value by eliminating the arterial plasma time–activity curve (TAC) arithmetically from model equations by using a TAC from a reference region where specific bindings are negligible, under the assumptions that the distribution volume of the nondisplacable compartment was equal in the target and reference regions, and that a target region can be described with the one-tissue compartment model shown in Eq. (1) (Lammertsma and Hume, 1996).

$$C_t(t) = R_1 C_r(t) + \left(k_2 - \frac{R_1 k_2}{1 + BP_{ND}}\right) e^{-\frac{k_2}{1+BP_{ND}}} \otimes C_r(t)$$
$$R_1 = K_1/K_1^r,\ BP_{ND} = k_3/k_4, \quad (1)$$

where C_t and C_r are the radioactivity concentrations in the target and reference regions, respectively, K_1 and K_1^r describe the rate constants for the transfer of radioligand from plasma to target and reference regions, respectively, k_2 describes the rate constant for the transfer of free radioligand from target region to plasma, and k_3 and k_4 represent the association and dissociation rate constants of the specific binding. This SRTM estimates three parameters, the delivery ratio of the target region to the reference region (R_1), the clearance rate constant of the target region (k_2), and binding potential, referred to as BP_{ND} by nonlinear least squares.

Table 2
Subjects and procedure of [^{11}C]FLB 457 study

Antipsychotic drug	Number of subjects	Age mean±SD	Dose of antipsychotic [mg]	Scan start time after antipsychotic administration [h]
Risperidon	5	28.6±6.2	2	4
Sultopride	3	25.3±2.3	25	2
Sulpiride	3	27.7±6.7	200	3

Receptor occupancy

Receptor occupancy is calculated from BP_{ND} of two scans, with and without antipsychotics, as follows:

$$\text{Occupancy}\ (\%) = 100^*(BP_{control} - BP_{drug})/BP_{control}, \quad (2)$$

where $BP_{control}$ represents the BP_{ND} value derived from a scan without antipsychotics and BP_{drug} represents that from a scan with antipsychotics (Farde et al., 1988).

Simulation study

Simulated TACs calculated for [^{11}C]raclopride and [^{11}C]FLB 457 with several BP_{ND} values and noise levels were generated to investigate the bias and variation of parameter estimates caused by statistical noise. Dynamic tracer concentrations for 90-min scans in the putamen of [^{11}C]raclopride and the temporal cortex of [^{11}C]FLB 457 were derived from Eq. (1) using a measured TAC of the cerebellum as a reference input function and assuming population mean input parameter values obtained previously in a study of untreated humans in which BP_{ND} values were varied to 100%, 50%, and 20% of the

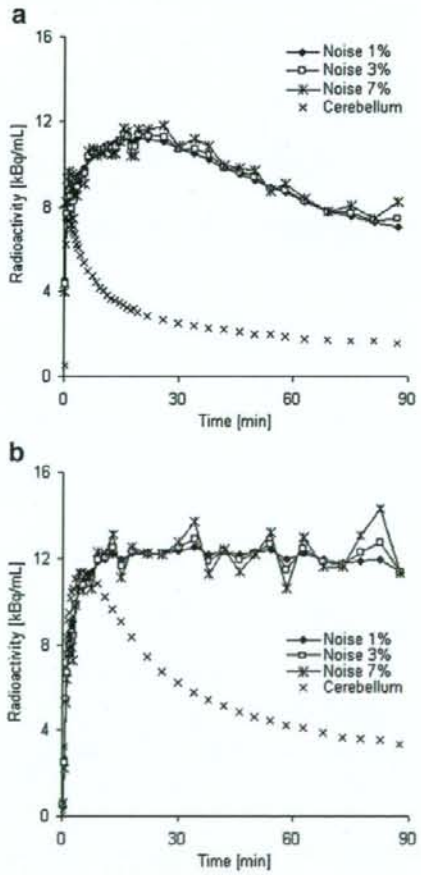

Fig. 1. Examples of simulated time–activity curves for the putamen with [^{11}C]raclopride (R_1=0.94, k_2=0.22, BP_{ND}=3.0) (a) and the temporal cortex with [^{11}C]FLB 457 (R_1=0.81, k_2=0.048, BP_{ND}=2.1) (b) at noise levels of 1%, 3%, and 7%. The time–activity curves for the cerebellum used as an input function were also shown.

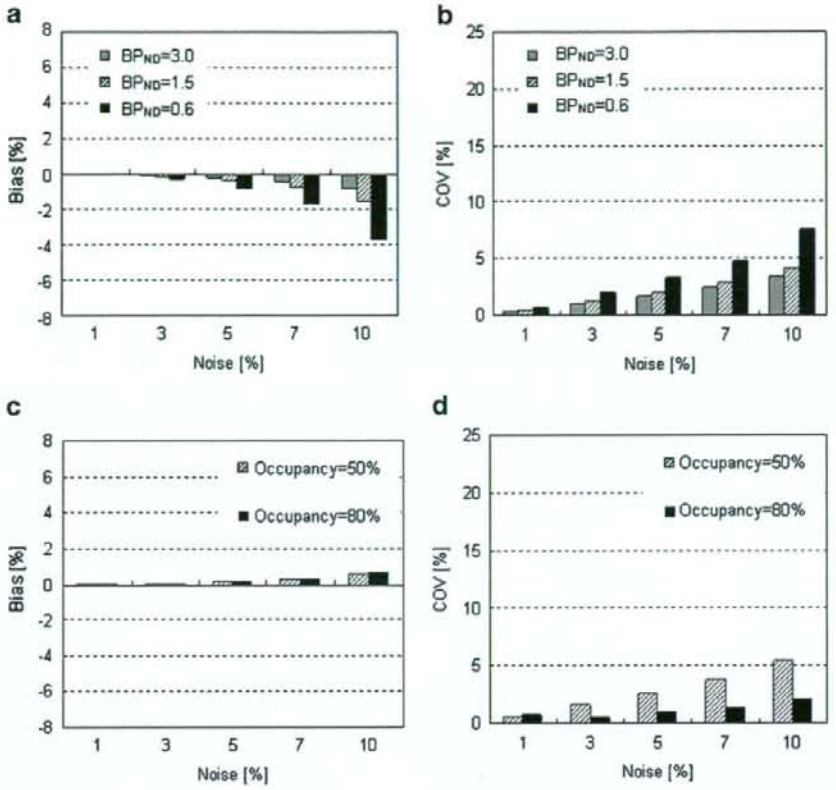

Fig. 2. Relation between noise level and reliability of BP_{ND} estimates (a, b) and between noise level and reliability of occupancy estimates (c, d) for simulated data of the putamen in [^{11}C]raclopride with R_1=0.94, k_2=0.22, BP_{ND}=3.0, 1.5 and 0.6 at noise levels of 1%, 3%, 5%, 7%, and 10%. Occupancy was calculated by BP_{ND} estimated from the time–activity curves with BP_{ND}=3.0 and 1.5 (occupancy=50%), and those with BP_{ND}=3.0 and 0.6 (occupancy=80%). Deducing from the residual error of TAC fitting by SRTM, the noise level of human ROI analysis was 1–5%.

original value (R_1=0.94, k_2=0.22, BP_{ND}=3.0, 1.5, and 0.6 for [^{11}C]raclopride, and R_1= 0.81, k_2= 0.048, BP_{ND}=2.1, 1.05, and 0.42 for [^{11}C]FLB 457).

The Gaussian-distributed mean-zero noise with variance proportional to the true TAC was added to the non-decaying tissue activity for each frame by Eq. (3) adopted from Logan et al. (2001).

$$SD\,(\%) = 100 \cdot \sqrt{N_i}/N_i, \tag{3}$$

$$N_i = \int_{t_i-\frac{\Delta t_i}{2}}^{t_i+\frac{\Delta t_i}{2}} C_t(t) \cdot e^{-\lambda t} \cdot dt \cdot F, \tag{4}$$

where i is the frame number, C_t is the non-decaying tissue radioactivity concentration derived from the k-values and the input function, t_i is the midpoint time of the ith frame, Δt_i is the data collection time, λ is the radioisotope decay constant, and F is a scaling factor representing the sensitivity of the measurement system, introduced here to adjust the noise level. It should be noted that this equation assumes that noise, which is added to the TAC, is determined by the count of the curve itself. In fact, noise is determined by the total counts in the slice, and is affected by random counts, dead time, etc. The level of noise for the dynamic data was expressed as the mean of percent SD described in Eq. (3) from 1 to 90 min. In this simulation study, F was chosen so that the level of noise would be 1, 3, 5, 7, and 10% for [^{11}C]raclopride and [^{11}C]FLB 457 TAC without BP_{ND} reduction, and one thousand noisy data sets were generated for each.

In these simulated TACs, kinetic parameters including BP_{ND} were calculated using the SRTM, and the relationship between the reliability of BP_{ND} estimates and noise level was investigated for TACs with various true BP_{ND}s. In these estimations, starting parameter values of the iteration for the fitting varied by ±25% from the true value (Ichise et al., 2003), and parameter estimates were considered invalid if R_1, k_2, BP_{ND} were negative or more than three times the true value. Occupancy was also calculated from Eq. (2) by using BP_{ND}s estimated from TACs with BP_{ND}=3.0 ([^{11}C]racloporide) or BP_{ND}=2.1 ([^{11}C]FLB 457) as $BP_{control}$ conditions. Reliability of the estimated parameters was evaluated by the bias of the mean value from the true value and coefficient of variation (COV; SD / mean[%]) of the estimates excluding outliers. In this evaluation, it was assumed that the TACs of [^{11}C]raclopride and [^{11}C]FLB 457 could be described with SRTM and that BP_{ND} estimated by SRTM represented binding potential estimated by a two-tissue compartment model with arterial input function.

Next, the effect of scan duration on BP_{ND} and occupancy estimates was investigated. In 90-min simulated TACs of 3%

noise level that corresponds to the noise level of human region-of-interest (ROI) analysis, the duration of the scan used for the fitting of parameter estimation was progressively reduced from 90 to 20 min for [^{11}C]raclopride and from 90 to 32 min for [^{11}C]FLB 457, and parameters were estimated by SRTM for each. The relationship between the reliability of parameter estimates and scan duration was evaluated by the COV of estimates and bias of the mean value from the true value for each fitting interval.

Human study

Subjects

Each of the [^{11}C]raclopride and [^{11}C]FLB 457 studies was based on eleven healthy male volunteers, some of whom were not the same in the two studies (Tables 1, 2). None of the subjects had a history of psychiatric, neurological, or somatic disorders, and none had alcohol- or drug-related problems. The study was approved by the ethics and radiation safety committees of the National Institute of Radiological Sciences, Chiba, Japan. Written informed consent was obtained from each subject.

Positron emission tomography procedure

For each subject, two PET scans were performed, before and after antipsychotic drug administration (Tables 1, 2), on separate days using the ECAT EXACT HR+ (CTI-Siemens, Knoxville, TN, USA), which provides 63 planes and a 15.5-cm axial field of view. A 10-min transmission scan with 3-rod source of ^{68}Ga–^{68}Ga was performed to correct for attenuation. Dynamic PET scans of [^{11}C]raclopride were carried out for 60 min (20 s×12, 60 s×16, 240 s×10) in 3-dimensional mode with a bolus injection of 217.3±14.1 MBq of [^{11}C]raclopride. The specific radioactivity was 198.9±54.4 GBq/μmol at the time of injection. PET scans of [^{11}C]FLB 457 were carried out for 90 min (20 s×9, 60 s×5, 120 s×4, 240 s×11, 300 s×6) in 3-dimensional mode with a bolus injection of 220.0±19.5 MBq of [^{11}C]FLB 457. The specific radioactivity was 174.7±48.1 GBq/μmol at the time of injection. There were no striking differences between the amount of cold raclopride or FLB 457 administered at baseline and after treatment of antipsychotic medication. Arterial blood sampling was not carried out in either study. All emission data were reconstructed by filtered-back projection using a Hanning filter with a cut-off frequency of 0.4 (full width at half maximum = 7.5 mm).

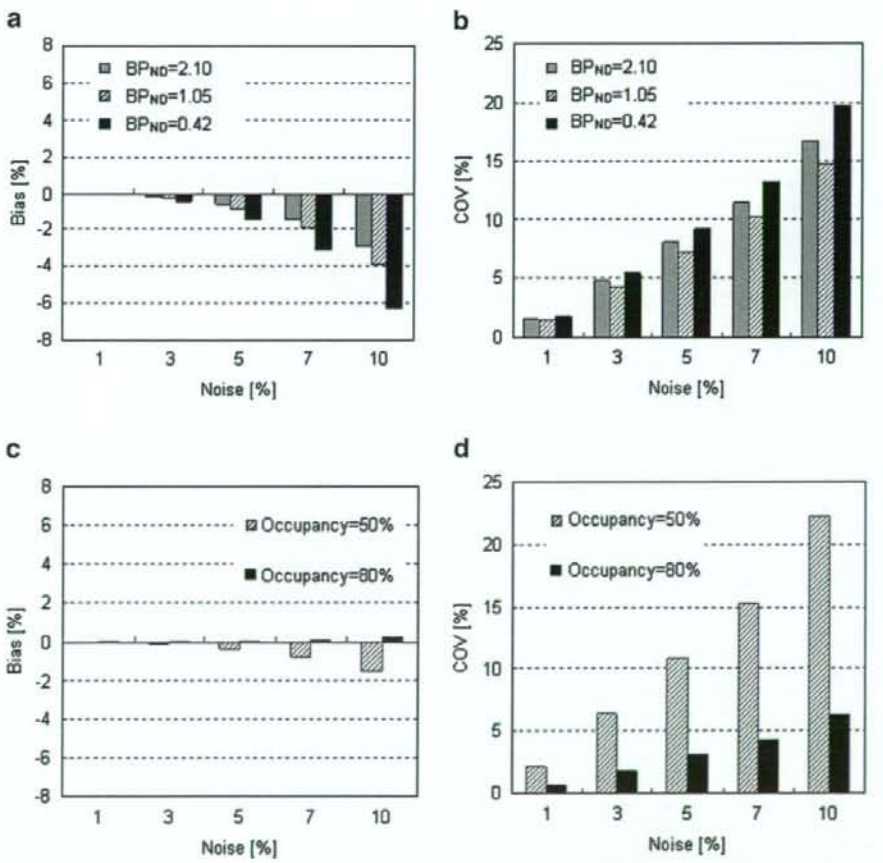

Fig. 3. Relation between noise level and reliability of BP_{ND} estimates (a, b) and between noise level and reliability of occupancy estimates (c, d) for simulated data of the temporal cortex with [^{11}C]FLB 457 with R_1 = 0.81, k_2 = 0.048, BP_{ND} = 2.1, 1.05 and 0.42 at noise levels of 1%, 3%, 5%, 7%, and 10%. Occupancy was calculated by BP_{ND} estimated from the time-activity curves with BP_{ND} = 2.1 and 1.05 (occupancy = 50%), and those with BP_{ND} = 2.1 and 0.42 (occupancy = 80%). Deducing from the residual error of TAC fitting by SRTM, the noise level of human ROI analysis was 1–5%.

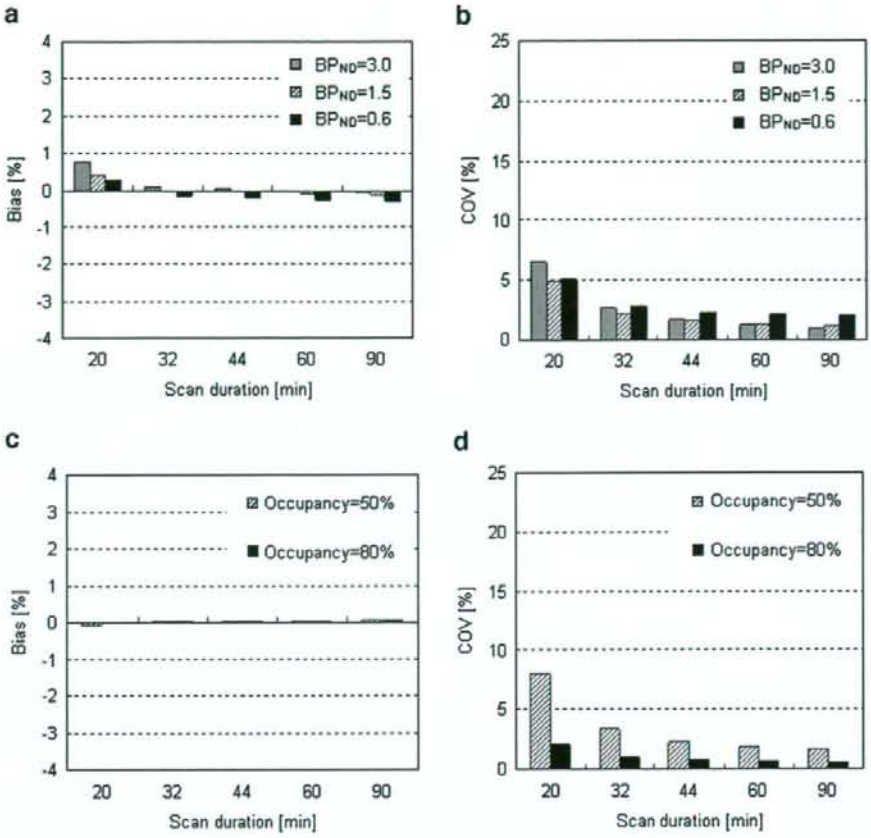

Fig. 4. Relation between scan duration and reliability of BP_{ND} estimates (a, b) and between scan duration and reliability of occupancy estimates (c, d) for simulated data of the putamen in [^{11}C]raclopride with R_1=0.94, k_2=0.22, BP_{ND}=3.0, 1.5, and 0.6 at a 3% noise level.

T1-weighted magnetic resonance imaging (MRI) of the brain was performed with Gyroscan NT, 1.5 T (Phillips Medical Systems, Best, The Netherlands).

Positron emission tomography data analysis

The summed PET images for all frames were coregistered to individual MR images, and ROIs were defined manually over the caudate, putamen, and cerebellum for [^{11}C]raclopride studies, and temporal cortex, thalamus, and cerebellum for [^{11}C]FLB 457 studies. In the TACs of these ROIs, R_1, k_2, and BP_{ND} were estimated by SRTM using the cerebellum as reference region, selected on the basis of its low specific binding (Olsson et al., 1999; Suhara et al., 1999).

In each scan, the reliability of parameter estimates was evaluated by a bootstrap approach with residual errors of fitting (Turkheimer et al., 1998; Kukreja and Gunn, 2004; Ogden and Tarpey, 2006). Briefly, weighted residual errors between measured and model-predicted TACs were calculated in each frame. Next, on the assumption that these errors of each frame $\varepsilon=[\varepsilon_1, \varepsilon_2, \varepsilon_3,..., \varepsilon_F]$ are independent, identically distributed, and of zero mean, resampled versions of the errors $\varepsilon^*=[\varepsilon_1^*, \varepsilon_2^*, \varepsilon_3^*,...,\varepsilon_F^*]$ were generated by random resampling of the original error ε. The resampling procedure for ε_i^* involved random selecting from ε with an equal probability associated with each of the F elements. Bootstrap replication TACs were generated by adding these resampling errors ε^* with appropriate weighting to the model-predicted TACs. In this study, the residual error of each frame was weighted with the SD derived from the TAC expressed as Eq. (3). It should be noted that the SD of each frame is not in a strict sense expressed by the counts of the TAC, as mentioned in the section above on Simulation study. Five hundred replication TACs were generated, parameters were estimated by SRTM for each, and mean and SD of these 500 estimates were calculated.

The relationship between the scan duration and COV of estimates and between the scan duration and bias was also investigated by shortening the interval of fitting of the bootstrap replication TACs from 60 to 20 min in [^{11}C] raclopride studies, and from 90 to 32 min in [^{11}C]FLB 457 studies. We define bias as the difference between the mean magnitude of BP_{ND} calculated for each truncated fitting interval and that of the 60-min fitting interval in [^{11}C] raclopride studies, and that of the 90-min fitting interval in [^{11}C]FLB 457 studies.

Analysis of simulation and human data was performed using Dr. View (AJS, Tokyo, Japan).

Results

Simulation study

Examples of simulated TACs for [^{11}C]raclopride and [^{11}C]FLB 457 with several noise levels and the cerebellum TAC used as reference input function are shown in Fig. 1. Deducing from the residual error of TAC fitting by SRTM, the noise level of human ROI analysis was about 1–5% in both [^{11}C]raclopride and [^{11}C]FLB 457 studies. BP_{ND} was estimated by SRTM using these simulated TACs, and occupancy was also calculated. In both [^{11}C]raclopride and [^{11}C]FLB 457 studies, the extent of the downward bias in BP_{ND} estimates became larger as noise increased or BP_{ND} decreased (Figs. 2a and 3a). However, in occupancy estimates, there was little bias even with a high noise level and with small occupancy (Figs. 2c and 3c). COV of BP_{ND} and occupancy became larger as noise increased (Figs. 2b, 2d, 3b, 3d). However, in both [^{11}C]raclopride and [^{11}C]FLB 457 studies, COV was under 6% at a 3% noise level. COV of occupancy estimates became larger when occupancy was smaller.

Next, the relationship between the reliability of BP_{ND} estimates, occupancy estimates, and scan duration was investigated. In [^{11}C]raclopride studies, there was little bias and COV was under 3% at a 3% noise level with both BP_{ND} and occupancy estimates with scan duration longer than 32 min (Fig. 4). Meanwhile, in [^{11}C]FLB 457 studies, COV was over 13% and bias from the 90-min scan became over 2% with BP_{ND} estimates when scan duration was shorter than 44 min (Figs. 5a, b). Although bias of occupancy estimates was small even if the scan duration became short, COV of occupancy estimates was also over 10% when occupancy was 50% and scan duration was shorter than 60 min (Figs. 5c, d). We had no outliers even when the scan duration was 20 min in [^{11}C]raclopride studies and when the scan duration was longer than 44 min in [^{11}C]FLB 457 studies.

Human study

An example of measured tissue-TACs at baseline and after administration of antipsychotic medication is shown in Fig. 6. The shape of the TACs was similar between before and after antipsychotic administration in the cerebellum, while the accumulation of radioactivity in the post-antipsychotic scan decreased at late times in other regions. Occupancies by antipsychotics were 27–79% with [^{11}C]raclopride and 18–86% with [^{11}C]FLB 457.

Bias and COV were estimated by a bootstrap approach. In the [^{11}C]raclopride studies there was no bias for either BP_{ND}

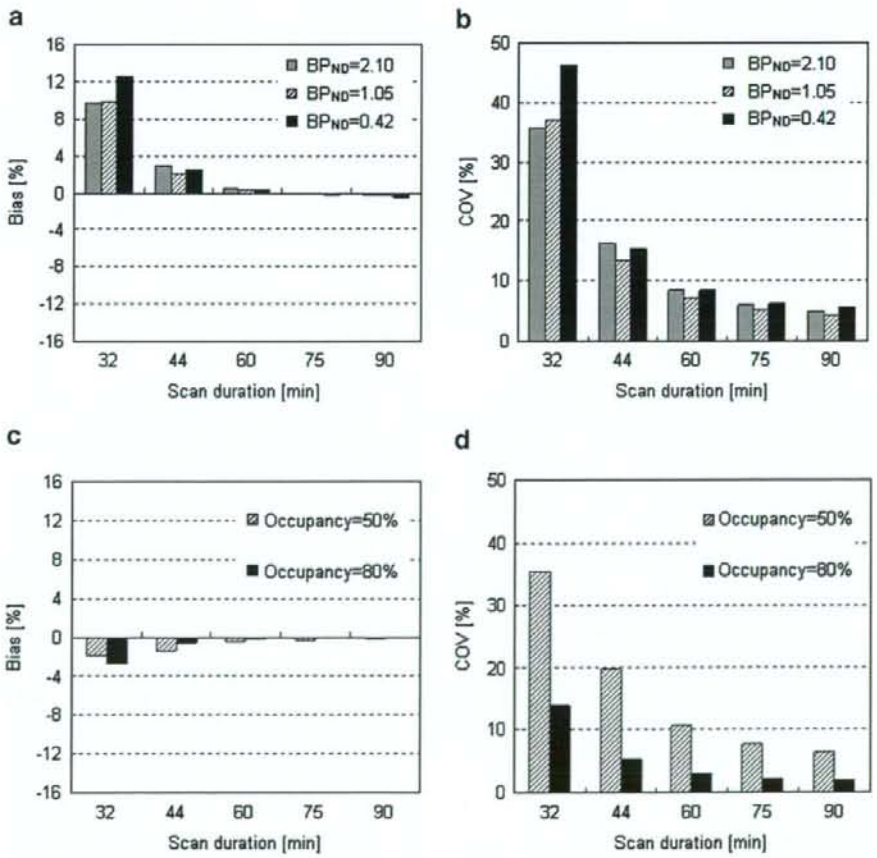

Fig. 5. Relation between scan duration and reliability of BP_{ND} estimates (a, b) and between scan duration and reliability of occupancy estimates (c, d) for simulated data of the temporal cortex in [^{11}C]FLB 457 with R_1=0.81, k_2=0.048, BP_{ND}=2.1, 1.05, and 0.42 at a 3% noise level.

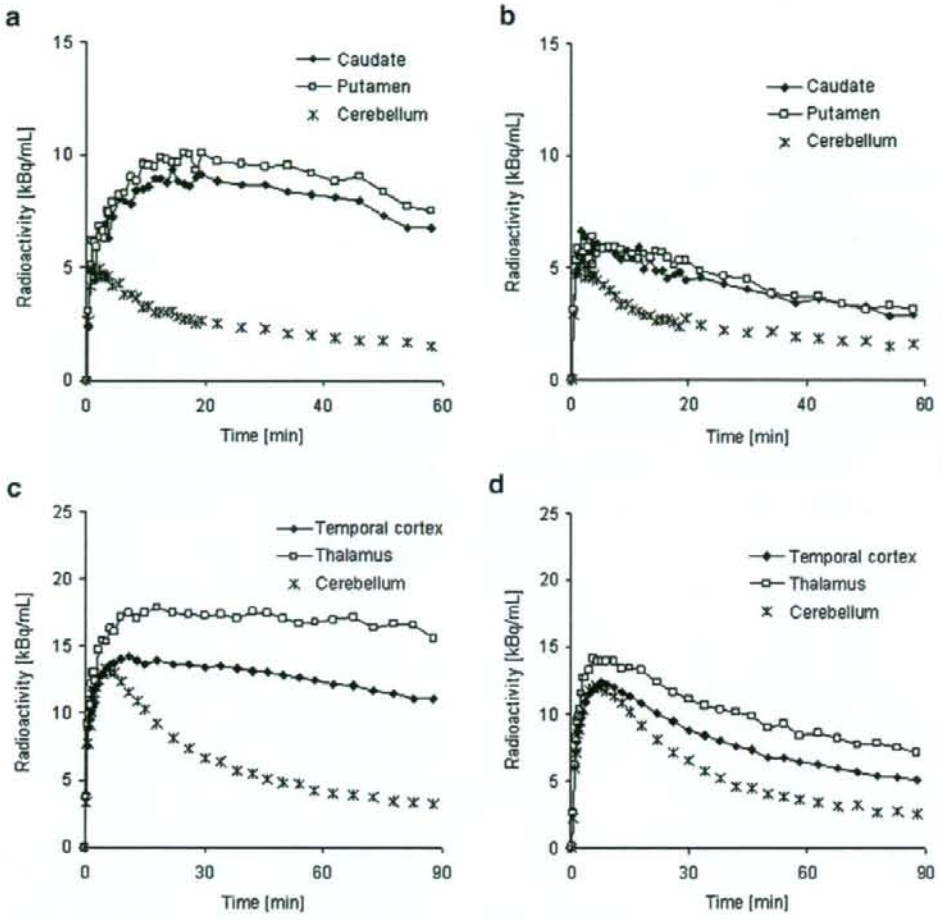

Fig. 6. Time–activity curves of pre-antipsychotic (left) and post-antipsychotic of risperidon (right) with [^{11}C]raclopride (a, b) and [^{11}C]FLB 457 (c, d). Occupancy of [^{11}C]raclopride was 71% in both the caudate and putamen, and that of [^{11}C]FLB 457 was 64% in the temporal cortex and 58% in the thalamus.

and occupancy estimates when scan duration was longer than 32 min. The COV in studies after antipsychotic administration were larger than that at baseline. When the scan duration was 32 min, COV of BP_{ND} was under 4% in the caudate and under 3% in the putamen at baseline, under 6% in the caudate and under 4% in the putamen after antipsychotic administration, and COV of occupancy was also under 6% in both regions (Figs. 7a, b). On the other hand, in [^{11}C]FLB 457 studies, the bias became larger when scan duration was shorter than 60 min. COV was about 5% for the 90-min scan, and when scan duration was shorter than 60 min, COV of BP_{ND} was greater than 9% in the thalamus, and greater than 5% in the temporal cortex at baseline, and greater than 13% in the thalamus, 9% in the temporal cortex after antipsychotic administration, whereas the COV of occupancy was also over 9% (Figs. 7c, d).

Discussion

In the quantification of receptor occupancy, it is necessary for binding potential to be quantified precisely before and after the administration of antipsychotics, since occupancy is derived from the binding potential values between these two scans. The simplified reference tissue model (SRTM) is often used in [^{11}C]raclopride and [^{11}C]FLB 457 studies. However, BP_{ND} varies widely in occupancy studies, and it can be difficult to obtain a solution for SRTM when specific binding is low, even given favorable noise levels (Gunn et al., 1997). Moreover, with a high noise level, the estimated parameters are affected by the noise in tissue TAC (Ichise et al., 2003). Therefore, in this study, we evaluated the effects of noise on the BP_{ND} estimates with SRTM for a range of BP_{ND} values likely to be encountered in occupancy studies with antipsychotic medication. As noise included in a reference TAC used as an input function may bring about an error in parameter estimates, in this study, the reference region was determined over the whole cerebellum, such that the resultant TAC is essentially noise-free.

On the other hand, Olsson and Farde simulated TACs with a plasma input curve and a two-tissue compartment model for various B_{max} values without noise and estimated occupancy by the peak equilibrium method, end time method, and SRTM (Olsson and Farde, 2001). They demonstrated that the drug occupancy estimated from SRTM was close to the assumed